Three-branched coumarin derivatives for two-photon uncaging. How does branching influence the efficacy?

Victor Dubois, Maxime Klausen, Jonathan Daniel, Frédéric Castet, Simon Plaize, Jean-Baptiste Verlhac, Mireille Blanchard Desce

Three-branched coumarin derivatives for two-photon uncaging. How does branching influence the efficacy?

Victor Dubois, Maxime Klausen, Jonathan Daniel, Frédéric Castet, Simon Plaize, Jean-Baptiste Verlhac,* Mireille Blanchard Desce*

Univ. Bordeaux, CNRS, Bordeaux INP, ISM, UMR 5255, F-33400 Talence, France.

In the design of non-linear optical chromophores, the conjugation pathways in multi-branched dyes are known to influence heavily their optical properties. Herein, we investigate this strategy for the design of two-photon (2P) responsive photolabile protecting groups (PPG) by assembling via a triphenylamine core extended coumarinylmethyl derivatives. The experimental study reveals an enhancement of the 2P absorption in the tri-branched compound, but a strikingly different photophysics behaviour resulting in a decrease in bond cleavage efficiency, and aggregation in aqueous acetonitrile. These combined effects results in much poorer 2P uncaging efficiency of the three-branched derivatives. In contrast, the corresponding mono-branched coumarin exhibit very high 2P photochemical efficiency (450 GM).

Keywords: Coumarins; Photorelease, Photosensitive Protecting Groups; Uncaging, Triphenylamine, Two-Photon Absorption

INTRODUCTION

Photoremovable Protecting Groups (PPGs) have recently found many applications in biology due to their ability to turn off a biomolecule of interest by a covalent linkage and to restore its bioactivity by suitable light irradiation.[1] Allowing accurate delivery of bioactive compounds, these smart photoactivatable molecules have widely contributed to several advances in opto-neurobiology.[2,3] In this context, various organic [4–7] and organometallic [8] molecules have recently been reported as PPGs owning the required criteria. As such, PPGs

must be stable in the dark, soluble in the biological media and the photolysis reaction - also known as "uncaging"[4] - must be clean, fast and ideally with high uncaging quantum yield (Φ_u).[1,9] The efficiency of the uncaging process also depends on the light-absorption capacity of the PPG at the wavelength of irradiation $\varepsilon(\lambda)$. For common one-photon (1P) excitation, the overall photosensitivity of the PPG is then defined as the product of both entities $\varepsilon_u = \varepsilon(\lambda).\Phi_u$ (in $M^{-1}.cm^{-1}$). Alternately, using multiphoton excitation provides critical advantages for photobiological applications, and especially for uncaging of biomolecules. These include increased penetration depth in biological tissues, *via* excitation in the biological spectral windows, i.e., 700-1000 nm and 1200-1600 nm. 2P excitation also permits highly confined 3D excitation of particular interest for neuroscientists. 2P excitation indeed allows delivery of neurotransmitters such as Glutamate (Glu) and Glycine (Gly) or γ-aminobutyric acid (GABA) with high spatial and temporal resolution (Olson et al., 2013; Shembekar et al., 2007; Trigo et al., 2009).

Similarly to the photosensitivity defined for 1P excitation, the efficiency of PPGs towards 2P excitation is quantified by the two-photon uncaging (2PU) cross-section (δ_u), defined as $\delta_u = \sigma_2.\Phi_u$ (in Goeppert-Mayer, 1 GM = 10^{-50} $cm^4.s^{-1}$), where σ_2 is the 2PA cross-section of the chromophore.[10] The 2PU sensitivity of a variety of popular PPGs has been investigated, showing that they show limited 2PU ability: methoxy-nitroindolines [6] ($\delta_u^{720\ nm}$ = 0.06 GM), *o*-nitroveratryle [5] ($\delta_u^{740\ nm}$ = 0.03 GM), bromo-hydroxy-quinoline [11] ($\delta_u^{740\ nm}$ = 0.59 GM) or bromo-hydroxy-coumarin[5] ($\delta_u^{740\ nm}$ = 0.72 GM). Such low values infer the use of high irradiation powers that are detrimental to the biological cells or tissues. In this sense, the required δ_u value for 50 % steady-state neurotransmitter uncaging was estimated to be 31 GM [12]. In this context, the need for more efficient 2P responsive PPGs has triggered very active research in the last two decades.[13–17] Among various PPGs, coumarinyl PPGs have

emerged as a suitable family of uncagers thanks to high Φ_u values, clean photolysis and fast photolytic reactions. The versatility of the coumarinyl backbone allows easy modification of the molecular structure of coumarinyl PPGs. Several attempts to enhance δ_u values either by playing on the push-pull system [18–21] and/or π-conjugated system [19,20,22,23] have been implemented giving rise to new coumarinyl PPGs. In this context, we recently demonstrated that very high δ_u values could be obtained by subtle tuning of the extent of intramolecular charge redistribution upon excitation in polarizable π-extended polar coumarinyl PPGs.[23] Following this route, we next aimed at extending this approach to branched systems. Indeed, it has long been known that multi-branched chromophoric systems could show high 2PA with significant σ_2 values. [24] Yet, the effect of branching on the 2PA properties depends on the nature of the various connecting nodes. Among them, the triphenylamine moiety has proven to be an efficient branching unit providing strong inter-branches coupling and major 2PA enhancement notably in the case of octupolar derivatives.[25] So far, the use of a triphenylamine donor core in PPGs was reported only for branched quinoline derivatives.[25,26]

We assumed that the use of a triphenylamine core would also be helpful for photolysis as it has been shown that the presence of an electron donor group at the 3-position of extended coumarinyl PPGs can influence positively the Φ_u value, in relation with the stabilization of the carbocation intermediate formed during photolysis.[20,27,28]

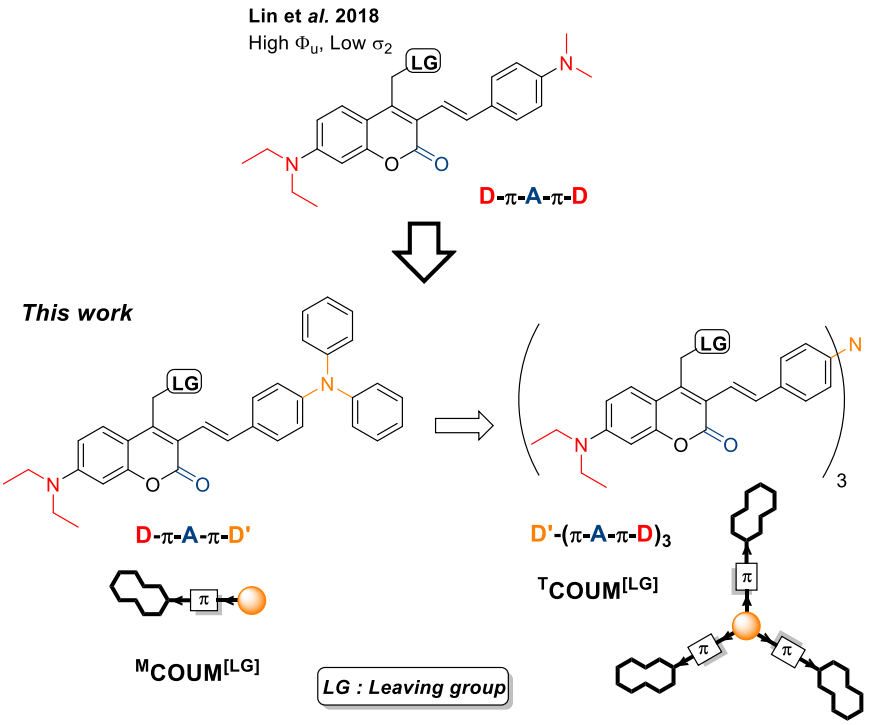

Figure 1. Structure of electron-rich mono- and multi-branched π-extended coumarin PPGs reported in previous and present work.

Based on these considerations, we thus decided to investigate how branching of extended coumarin cages onto the triphenylamine donor core could influence their 2P photolysis ability (Figure 1). We hereby describe the synthesis, photophysical and photochemical properties of trimeric coumarinyl derivatives (**^{T}COUM)** and of its monomeric analogues (**^{M}COUM)**.

RESULTS AND DISCUSSION

Synthesis

The trivinylphenylamine core **4** was first synthesized by Kumada-Corriu cross-coupling while its mono-vinyl analogue was obtained by Wittig reaction starting from the commercially available aldehyde **1**. The key halogenated coumarin **6** was obtained in four steps following the convenient selenium-free pathway recently reported and starting from the commercially available 7-diethylamino-4-methylcoumarin.[23,29] Both **^{M}COUM$^{[OH]}$** and **^{T}COUM$^{[OH]}$** were

then synthesized by reacting the appropriate vinyl compound and **6** in a Heck cross-coupling performed in Jeffery's conditions.[30] Fluorenylmethyloxycarbonyl (Fmoc)-protected glycine (Gly-Fmoc) was finally chosen as the leaving group of our new PPGs. Indeed, the Fmoc group (a common protecting group for amine functions) absorbs UV-light allowing us to follow the photorelease of glycine by RP-HPLC follow-up. To this end, Gly-Fmoc was introduced on both compounds by typical Steglich [31] esterification to give **^{T}COUM$^{[Gly-Fmoc]}$** and **^{T}COUM$^{[Gly-Fmoc]}$** with reasonable yields (Scheme 1).

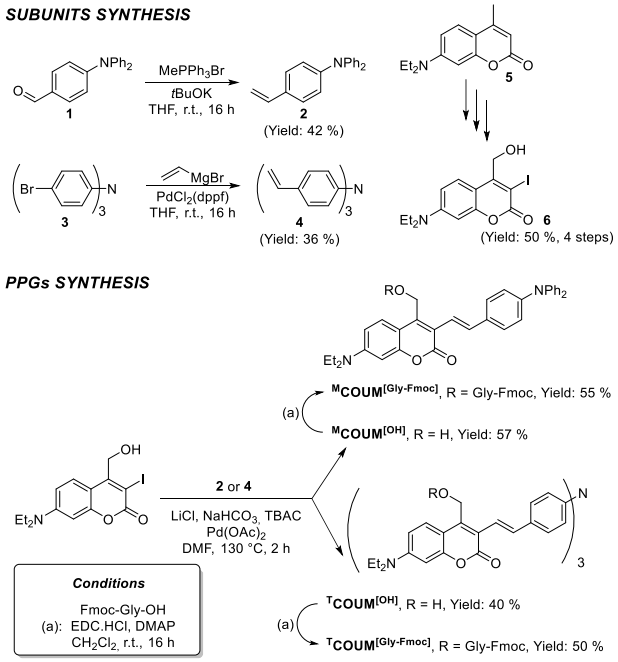

Scheme 1. Synthetic route to ^{M}COUM$^{[Gly-Fmoc]}$ and ^{T}COUM$^{[Gly-Fmoc]}$.

Photophysical properties

The photophysical properties of both the free derivatives **^{M}COUM$^{[OH]}$** and **^{T}COUM$^{[OH]}$** and the caged GlyFmoc were investigated in different solvents (Table 1). All compounds show an intense absorption band in the blue visible range, similar to π-extended coumarins previously described in the literature.[19,20,32,33].

Table 1. Photophysical properties of free [OH]-PPGs ^{M}COUM$^{[OH]}$ and ^{T}COUM$^{[OH]}$, and caged compounds ^{M}COUM$^{[Gly\text{-}Fmoc]}$ and ^{T}COUM$^{[Gly\text{-}Fmoc]}$.

Cpd	Solvent	λ_{abs}^{max} (nm)	λ_{em}^{max} (nm)	ε^{max} (M-1.cm-1)	Φ_f [a]	λ_{2PA}^{max} (nm)	σ_2 [b] (GM)
^{M}COUM$^{[OH]}$	THF	433	518	4.4 10^4	0.76	730	900
	MeCN	435	537	4.2 10^4	0.72	750	580
	DMSO	443	535	4.5 10^4	0.79	740	600
	Aq. MeCN[c]	436	548	4.0 10^4	0.48	730	840
^{T}COUM$^{[OH]}$	THF	449	539	1.1 10^5	0.52	750	2700
	MeCN	450	546	1.1 10^5	0.02		
	DMSO	458	564	1.1 10^5	0.03	760	2100
	Aq. MeCN[c]	451	549		<0.01		
^{M}COUM$^{[Gly\text{-}Fmoc]}$	THF	445	531	4.4 10^4	0.73		
	Aq. MeCN[c]	447	570	4.5 10^4	0.28		
^{T}COUM$^{[Gly\text{-}Fmoc]}$	THF	462	566	9.0 10^4	0.31		
	MeCN	460	566		0.01		
	DMSO	468	574	1.1 10^5	0.02		
	Aq. MeCN[c]	463	569	7.5 10^4	<0.01		

[a] Fluorescence quantum yield. Standard: fluorescein in 0.1 M NaOH (Φ_f = 0.9). [b] Two-photon absorption cross-section at λ_{2PA}^{max} derived from 2PEF experiments (1 GM = 10^{-50} $cm^4.s^{-1}$). [c] MeCN/H_2O (9/1, v/v).

As observed from Figure 2, the branching leads to a noticeable red-shift as well as a slight decrease (when normalized with respect to the number of branches) and a broadening of the absorption band. A shoulder is clearly observed around 400 nm in the case of trimeric derivatives, indicative of the presence of a close higher excited state. On the other hand, the absorption bands remain relatively unaffected by the change of solvent polarity (Figure 3).

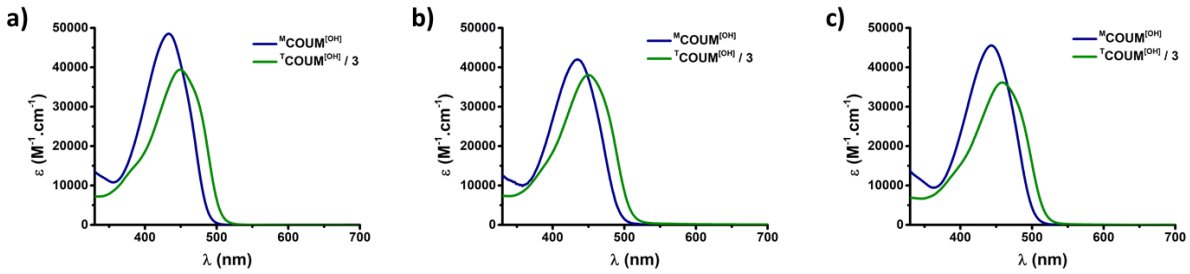

Figure 2. Comparison of the absorption spectra of ^{M}COUM$^{[OH]}$ and ^{T}COUM$^{[OH]}$ (normalized by the number of branches) in a) THF, b) MeCN, c) DMSO.

Both compounds show bright green fluorescence in THF, i.e. in a medium polarity solvent, which is slightly red-shifted in polar solvents such as acetonitrile or DMSO or in aqueous acetonitrile (Figure 3).

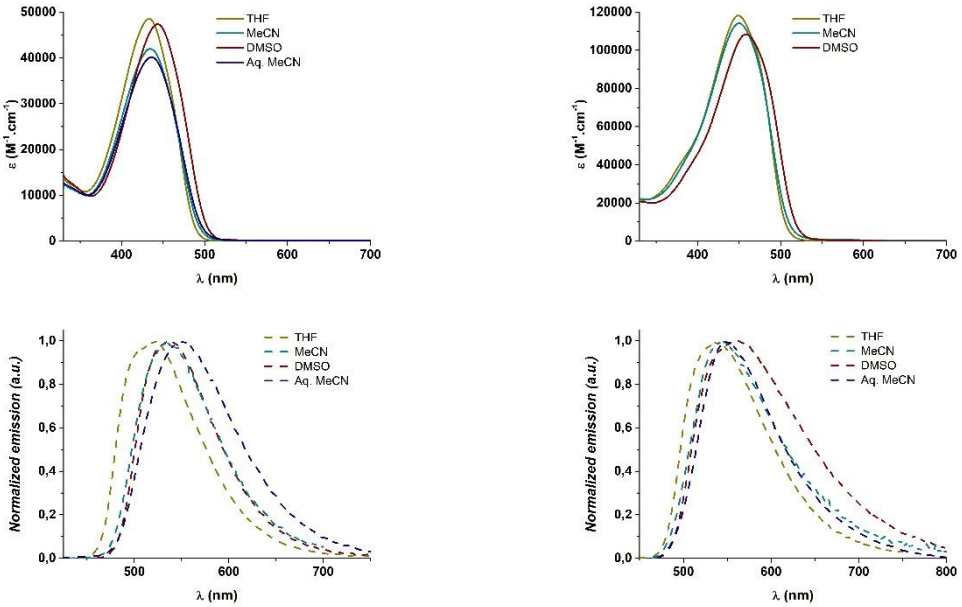

Figure 3. Effect of solvent polarity on the absorption (top) and emission of ^{M}COUM$^{[OH]}$ (left) and ^{T}COUM$^{[OH]}$ (right)

Interestingly, we note that **^{M}COUM$^{[OH]}$** retains sizeable fluorescence in high polarity solvents, while **^{T}COUM$^{[OH]}$** shows vanishing fluorescence in polar solvents (Table 1). The high fluorescence of compound **^{M}COUM$^{[OH]}$** in polar solvents indicates that this extended coumarin does not undergo TICT (twisted intramolecular charge transfer), [34] most probably in relation

with the electron-donating effect of the diphenylamino end-group, which destabilizes the TICT state. In contrast, **^{T}COUM$^{[OH]}$** retains fluorescence only in a low polarity solvent (THF) and shows diminishing fluorescence in aqueous acetonitrile. This suggests that an efficient non-radiative deactivation process occurs in the excited state of **^{T}COUM** in polar solvents. Such competitive process may represent a hurdle for the photolysis of the tripodal cage **^{T}COUM$^{[Gly-Fmoc]}$** as it can provides a competitive deactivation channel once the first Gly unit has been released, hindering the subsequent release of the two remaining Gly units. Finally, we stress that **^{M}COUM$^{[Gly-Fmoc]}$** shows diminished fluorescence quantum yield in aqueous acetonitrile as compared to the free cage **^{M}COUM$^{[OH]}$** suggesting that uncaging is indeed operative.

Theoretical calculations

As shown on Figure 4, the shapes of the highest occupied and lowest unoccupied molecular orbitals (HOMO and LUMO) reveal an intramolecular charge redistribution from the donor terminal groups towards the centre of the molecule for the monomeric derivative **^{M}COUM**, while the trimeric derivative **^{T}COUM** shows related behaviour along each of its branch. This photo-induced charge transfer is also evidenced by the variation of the total electron density from the ground (S_1) to the lowest-energy excited state (S_2) in **^{M}COUM**, and to the two degenerate excited states S_1 and S_2 in **^{T}COUM** (Figure 4). We note that this charge redistribution is reminiscent of that reported for branched systems built from a triphenylamine core and quadrupolar arms. [35]

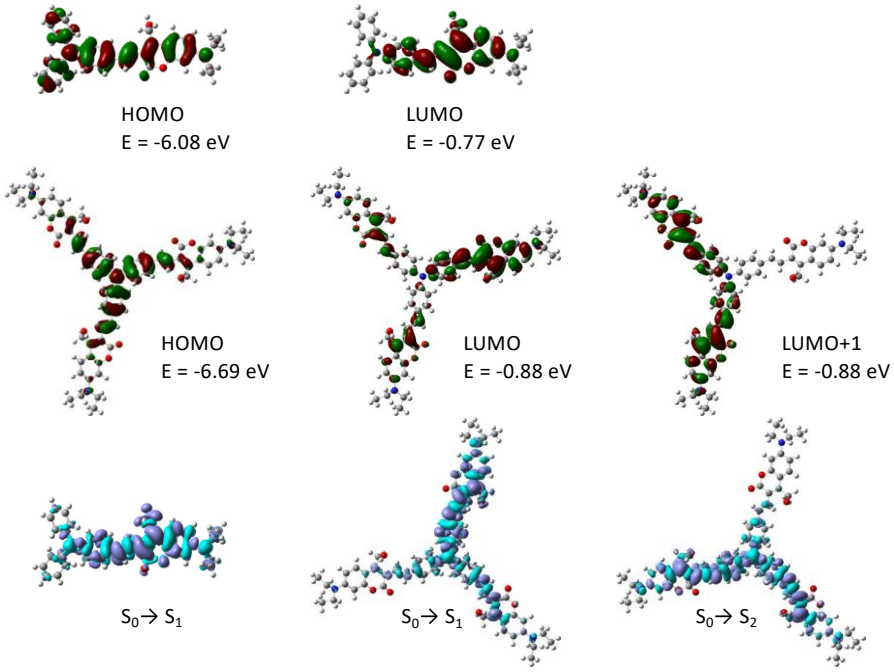

Figure 4. Isodensity plots of the frontier molecular orbitals of ^{M}COUM$^{[OH]}$ (top) and ^{T}COUM$^{[OH]}$ (middle), and electron density differences associated to the lowest-energy electronic transitions (bottom) for the two chromophores.

The energies (ΔE) and oscillator strengths associated to the lowest-energy electronic transitions, as well as the quantities characterizing the spatial extent of the photo-induced charge transfer in both compounds (Le Baher et al, 2011; Ciofini et al, 2012), namely, the amount of charge transferred Δq, the charge transfer distance Δr and the dipole moment variation $\Delta \mu$, are gathered in Table 2.

Table 2: **Vertical $S_0 \rightarrow S_1$[(a)] transition energy (ΔE_{01}, eV), wavelength (λ_{01}, nm), oscillator strength (f_{01}, dimensionless), as well as ground and excited state dipole moments (μ_0 and μ_1, D), dipole moment variation ($\Delta\mu_{01}$, D), charge transferred upon excitation (Δq, |e|), and charge transfer distance (Δr, Å).**

Compound	ΔE_{01}	λ_{01}	f_{01}	μ_0	μ_1	$\Delta\mu_{01}$	Δq	Δr
^{M}COUM$^{[OH]}$	3.10	400	1.96	8.07	6.94	1.16	0.56	0.43
^{T}COUM$^{[OH]}$ [(a)]	2.93	423	2.74	7.84	8.34	3.89	0.57	1.42

[(a)] For the **^{T}COUM$^{[OH]}$** derivative, the S_1 and S_2 states are degenerate and have the same electronic properties.

Consistently with UV-vis measurements and the reduction of the HOMO-LUMO gap (5.31 vs 4.81 eV, see Figure 4 for the orbital energies), TD-DFT calculations predict a red-shift of the main absorption band of **^{T}COUM** compared to its monomeric analogue. The slight decrease in the intensity of the absorption band normalized by the number of branches is also well reproduced by the lowering of the normalized oscillator strengths ($f_{01} = 1.96$ for **^{M}COUM** and $(f_{01} + f_{02})/3 = 1.82$ for **^{T}COUM**). The photo-induced reorganization of the electron density illustrated in Figure 4 is further quantified by the increase of dipole moment upon excitation. In **^{M}COUM**, the dipole moment variation is relatively weak ($\Delta\mu_{01}$~1 D), according to the small charge transfer distance ($\Delta r = 0.43$ Å) resulting from the pseudo-quadrupolar nature of the molecule. A slightly larger $\Delta\mu_{01}$ value is calculated in the C_3-symmetrical **^{T}COUM** derivative, in which the intramolecular charge transfer occurs perpendicularly to the main molecular plane.

Two-photon absorption

The 2PA spectra of both monomeric and branched compounds were determined by conducting two-photon excited fluorescence (2PEF) experiments on the free ([OH]) derivatives **^{M}COUM$^{[OH]}$** in various solvents and on **^{T}COUM$^{[OH]}$** in THF. These compounds do not undergo

photolysis and retain suitable fluorescence in the selected solvents, thus permitting reliable 2PEF measurements (Figure 5.).

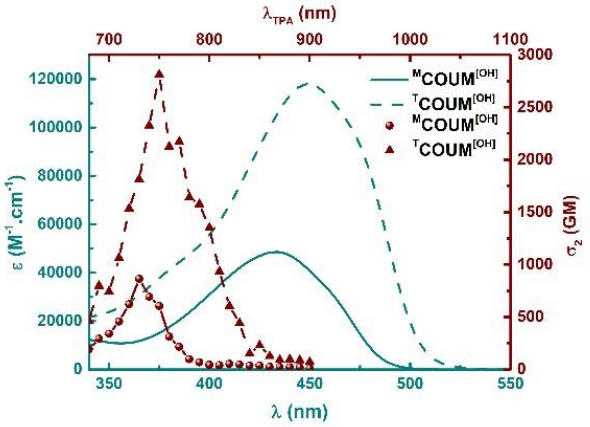

Figure 5. 1PA vs 2PA of ^{M}COUM$^{[OH]}$ (solid line) and ^{T}COUM$^{[OH]}$ (dotted line) in THF.

Both compounds show an intense 2PA band in the NIR1 region peaking around 750 nm (Figure 5). We note that the 2PA response of **^{M}COUM$^{[OH]}$** is large (with σ_2^{max} values ranging between 600 and 900 GM depending on the solvent), comparable to that of extended coumarins having both an extended π-conjugated and an electron-withdrawing endgroup [23]. **^{M}COUM$^{[OH]}$** shows an even larger 2PA response than the prototypical derivative by Lin et *al.* (Figure 1), evidencing the marked positive influence of the diphenylamine end-group as compared to the diethylamino or even julolidine moiety.[20] The large σ_2^{max} value of **^{M}COUM$^{[OH]}$** may be related to its dissymmetrical "pseudo-quadrupolar" nature D-π-A-π-D'. This is clearly noticeable from Figure 6: the lowest one-photon allowed excited state is almost two-photon forbidden whereas a higher almost one-photon forbidden excited state is responsible for the 2PA response of both **^{M}COUM$^{[OH]}$** and **^{T}COUM$^{[OH]}$**. We note that **^{T}COUM$^{[OH]}$** shows a much broader 2PA band than **^{M}COUM$^{[OH]}$** and a slightly red-shifted peak. The 2PA maximum cross-sections of **^{T}COUM$^{[OH]}$** is about three times that of the monomeric compound **^{M}COUM$^{[OH]}$** (both in THF and DMSO), indicating an almost linear behaviour in terms of 2PA response as a function of the size. Such behaviour is consistent with earlier reports

on the 2PA response of branched systems built from a triphenylamine core and quadrupolar arms.[35] Yet we point out that the branching has a marked influence on the 2PA range as **^{T}COUM$^{[OH]}$** maintain high 2PA response at 800 nm while **^{M}COUM$^{[OH]}$** shows only vanishing 2PA at that wavelength (Figure 5). Here again, such behaviour is similar to what was reported for branched systems built from a triphenylamine core and quadrupolar arms [35].

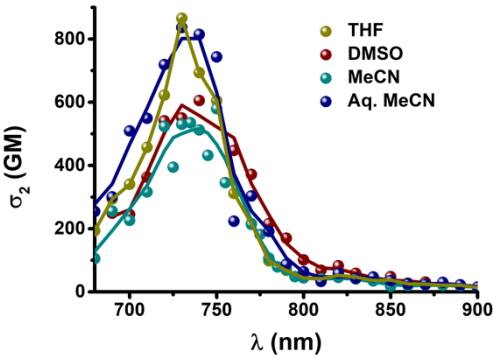

Figure 6. Two-photon absorption spectra of ^{M}COUM$^{[OH]}$ in different solvents.

We note that the solvent polarity affects the 2PA spectra of ^{M}COUM$^{[OH]}$. As illustrated in Figure 6, a broadening and significant reduction of the 2PA band is observed upon going from a low-medium polarity solvent (THF) to polar aprotic solvents (MeCN or DMSO). In contrast, an intense 2PA band is restored in protic environments.

Photochemical properties

The uncaging properties have then been investigated by performing 1P photolysis of both **^{M}COUM$^{[Gly\text{-}Fmoc]}$** and **^{T}COUM$^{[Gly\text{-}Fmoc]}$** in aqueous acetonitrile. For comparative purposes, the photolysis of a reference compound DEAC450 (Figure 7) [19,23] was performed in the strict same conditions (see Materials and Methods).

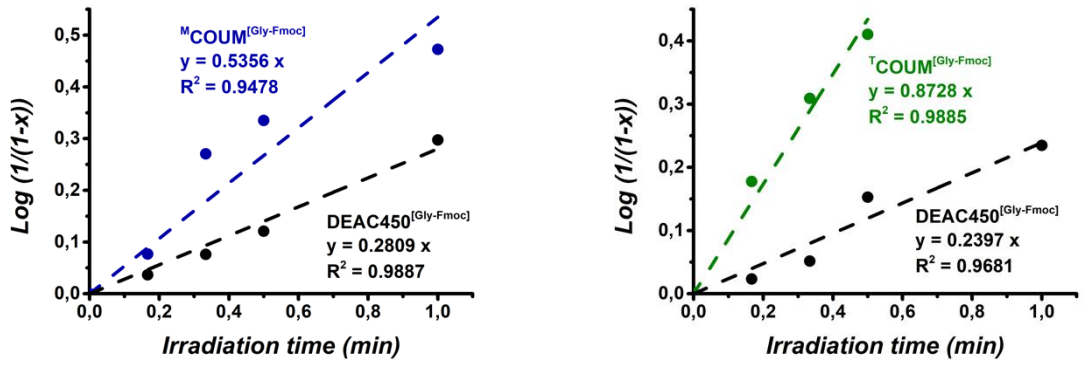

Figure 7. Comparative kinetics of photolysis upon irradiation at 455 nm of the reference PPG (DEAC450 ; Φ_u = 0.39) and of ^{M}COUM$^{[Gly\text{-}Fmoc]}$ and ^{T}COUM$^{[Gly\text{-}Fmoc]}$ In the y axis, x corresponds to the conversion (i.e. fraction of free Gly-Fmoc with respect to caged Gly-Fmoc).

The photolysis was monitored by RP-HPLC following the release of free Fmoc-Gly-OH (See ESI). First-order kinetics (Figure 7) allowed the derivation of the 1P uncaging sensitivity ($\varepsilon_{455}.\Phi_u$). [23].

Table 3. Photochemical properties of caged PPGs ^{M}COUM$^{[Gly\text{-}Fmoc]}$ and ^{T}COUM$^{[Gly\text{-}Fmoc]}$ in aqueous acetonitrile (9:1).

Cpd	$\varepsilon_{455\ nm}$ ($M^{-1}.cm^{-1}$)	Q_u/Q_u^{ref} a)	Q_u^{rel} b)	ε_u^{max} c) ($M^{-1}.cm^{-1}$)	δ_u^{max} d) (GM)
^{M}COUM$^{[Gly\text{-}Fmoc]}$	$4.4.10^4$	1.38	0.54	$2.4.10^4$	450
^{T}COUM$^{[Gly\text{-}Fmoc]}$	$7.3.10^4$	0.56	0.22	$1.6.10^4$	-

a) Ratio of uncaging quantum yield values derived from comparative 1P photolysis experiment in CH_3CN/H_2O (9/1, v/v) at 455 nm. b) Uncaging quantum yield values calculated using $\Phi_u^{ref} = 0.39$ for DEAC450$^{[Gly\text{-}Fmoc]}$. c) 1P uncaging sensitivity at λ^{max}. d) 2P uncaging sensitivity at Φ_{2PA}^{max} estimated from comparative 1P photolysis experiments and 2PEF measurements conducted in aqueous acetonitrile.

Results are gathered in Table 3. **^{M}COUM$^{[Gly\text{-}Fmoc]}$** exhibits a substantial Φ_u value (54 %), superior to that DEAC450 PPG [19] and in perfect agreement with the effect of stronger electron-donating substituents reported by Lin et al.[20] In addition, UV-Vis follow-up of

^{M}**COUM**$^{[Gly\text{-}Fmoc]}$ photolysis reaction clearly shows the decrease of the absorption band located at 447 nm and the appearance of a new absorption band at 387 nm (Figure 8.). This new band matches perfectly with the absorption band of DEAC which is consistent with the formation of a cyclized DEAC-type photolysis by-product as reported by Lin *et al.* [20]

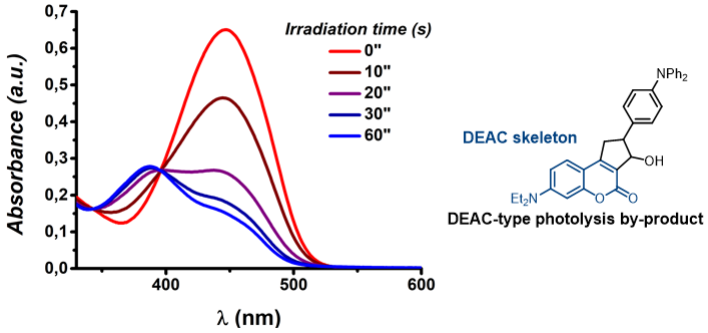

Figure 8. UV-Vis follow-up of the photolysis reaction of ^{M}COUM$^{[Gly\text{-}Fmoc]}$.

Strikingly, the three-branched derivative ^{T}**COUM**$^{[Gly\text{-}Fmoc]}$ shows a much smaller uncaging quantum yield than ^{M}**COUM**$^{[Gly\text{-}Fmoc]}$. We stress that the Φ_u value of ^{T}**COUM**$^{[Gly\text{-}Fmoc]}$ has been calculated with respect of 3 equivalent release of Gly-Fmoc. The decrease of the overall Φ_u value may possibly be attributed to the different kinetics of the sequential release of the three Gly-Fmoc moieties. In particular, the competing deactivation process that is responsible for the fluorescence quenching of ^{T}**COUM**$^{[OH]}$ in polar environments may indeed play an important role as it might indeed compete effectively with the photolysis of intermediates ^{T}**COUM**$^{[2(Gly\text{-}Fmoc)(OH)]}$ and ^{T}**COUM**$^{[(Gly\text{-}Fmoc)2(OH)]}$, thus reducing the overall uncaging efficiency.

In order to further assess the uncaging efficiency of the monomeric and trimeric cages under 2P excitation, we then performed 2P photolysis experiments in solution. Experiments were conducted at 750 nm (i.e. near the 2PA maxima) in aqueous acetonitrile using DEAC$^{[Gly\text{-}Fmoc]}$ as a convenient benchmark as its 2PA maxima is close to 750 nm. As seen in Figure 10,

the percentages of photoreleased Gly-Fmoc after irradiation at 750 nm in the exact same conditions show that **^{M}COUM$^{[Gly\text{-}Fmoc]}$** is clearly by far the most effective 2P-PPG and more efficient than DEAC$^{[Gly\text{-}Fmoc]}$. In contrast, **^{T}COUM$^{[Gly\text{-}Fmoc]}$** appears as only slightly more efficient than DEAC450$^{[Gly\text{-}Fmoc]}$. The reduced overall uncaging quantum yield does not account for all of the loss in 2P uncaging efficiency. Based on the observation that **^{T}COUM$^{[Gly\text{-}Fmoc]}$** shows dramatically lower solubility than **^{M}COUM$^{[Gly\text{-}Fmoc]}$**, we suspected that **^{T}COUM$^{[Gly\text{-}Fmoc]}$** may partially aggregate in aqueous acetonitrile. To test this hypothesis, we performed single particle analysis using the same concentration as used for 1P and 2P photolysis experiments (i.e. in the μM range). Indeed, small particles could be noted revealing that the three-branched compound self-assembles in aqueous acetonitrile (See SI).

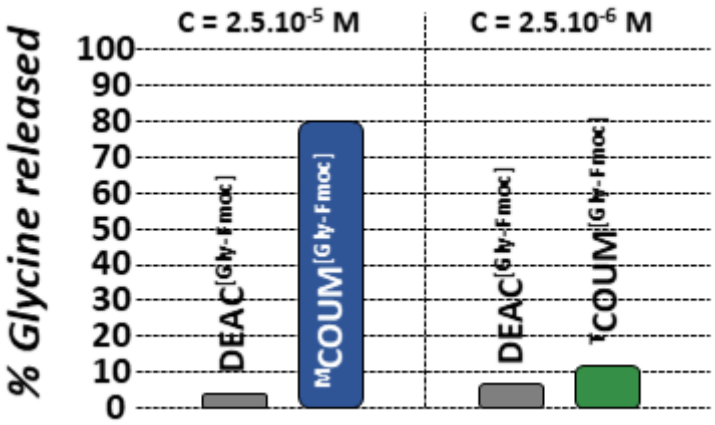

Figure 10. Histogram of the 2P photolysis showing the percentage of Gly-Fmoc released after 4 h of irradiation at 750 nm (1 W, volume of 1.2 mL CH_3CN/H_2O 9:1).

The present study clearly shows that the direct branching strategy of three coumarinyl cages via a triphenylamine core does not appear as a beneficial one for 2P uncaging. However, this does not arise from the 2PA response of the isolated trimeric compound but may be ascribed to its aggregation in aqueous environments.

CONCLUSION

To summarize, we have shown that multimeric branched structures built from a triphenylamine core could lead to PPGs with high 2PA cross-section. Yet, the branching has a marked detrimental effect on the 2P uncaging efficiency in aqueous mixtures. This reduced 2PU ability stems both from a decrease of the uncaging efficiency (related to a competitive deactivation process occurring in the excited state) and from the self-aggregation of the three-branched derivative in aqueous mixtures. In contrast, the monomeric D-π-A-π-D' structure (**^{M}COUM**) was found to be a most promising PPG owing to its high 2PA cross-section and good uncaging quantum yield, yielding an exceptional estimated δ_u value (~450 GM) in aqueous acetonitrile. The triphenylamine end-group not only conveys a higher 2PA response than most extended coumarinyl PPG, but also induces appreciable uncaging efficiency, leading to reasonable ε_u and unprecedented δ_u values. In addition, this compound also shows clean photolysis and excellent dark stability (See ESI). This study thus paves the way to unique opportunities for efficient and highly localized delivery of bioactive molecules. Further work along that direction is currently in progress, especially aiming at addressing the crucial point of large solubility in biological aqueous media.

EXPERIMENTAL SECTION

General details of synthesis materials, of spectroscopic measurements, of uncaging quantum yield measurements (Φ_u), of 1- and 2-photon photolysis and of 2-photon absorption experiments have been previously described [23] and will only be briefly recalled in the ESI. Characterization data (^{1}H and ^{13}C NMR spectra) for all compounds as well as 1- and 2-photon absorption spectra and RP-HPLC chromatograms can also be found in the ESI.

Synthetic procedures

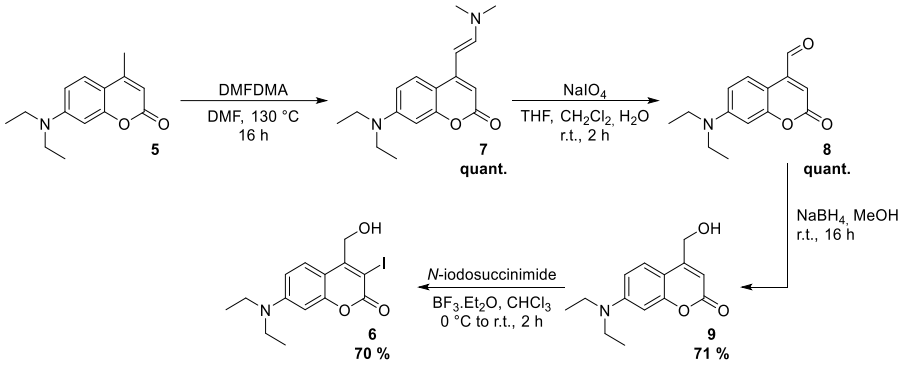

Scheme 2. Synthetic pathway to the 3-halogenated coumarin 6.

tris(4-vinylphenyl)amine (4). Compound **3** (1.00 g, 2.07 mmol, 1 eq.) was dissolved in dry THF under argon atmosphere and argon was bubbled into the mixture for 20 minutes. $PdCl_2$dppf (8 mg, 82.8 µmol, 0.05 eq.) was then added before a solution of vinylmagnesium bromide (897 mg, 6.84 mmol, 3.3 eq.) in dry THF was added dropwise. Argon was finally bubbled into the mixture for 5 more minutes and the resulting mixture was stirred overnight at room temperature. Water was added and the mixture was extracted with petroleum ether. The combined organic layers were then dried with Na_2SO_4, filtered over Celite® and concentrated. The crude was purified by column chromatography of silicagel (eluent: petroleum ether, 100 %) to give the pure compound **4** as a white solid (230 mg, 36 %). **R_f (*TLC conditions:* PE, 100 %)**: 0.40 (Rev: UV). **^{1}H NMR (300 MHz, Chloroform-*d*) δ (ppm)** 7.31 (d, *J* = 8.6 Hz, 6H), 7.05 (d, *J* = 8.6 Hz, 6H), 6.67 (dd, *J* = 17.6, 10.9 Hz, 3H), 5.66 (dd, *J* = 17.6, 1.0 Hz, 3H), 5.18 (dd, *J* = 10.9, 1.0 Hz, 3H). **^{13}C NMR (76 MHz, $CDCl_3$) δ (ppm)** 147.0, 136.2, 132.4, 127.1, 124.1, 112.4. **HRMS (ESI)**: m/z = 324.17436, calcd for $C_{24}H_{22}N$ $(M+H)^+$: 324.17468 **FTIR ν (cm^{-1}):** 2959.2, 2919.7, 2850.3, 1595.8, 1501.3, 1322.9, 1307.5, 1275.7, 1178.3, 987.4, 838.9. **Melting point:** 101 °C.

(E)-7-(diethylamino)-4-(2-(dimethylamino)vinyl)-2*H*-chromen-2-one (7) was synthesized according to the procedure described in the literature [23] and obtained as a yellow

297 powder (24.6 g, quant.). Analytical data were in accordance with the literature. **^{1}H NMR (300**
298 **MHz, $CDCl_3$) δ (ppm):** 7.51 (d, *J* = 9.1 Hz, 1H), 7.20 (d, *J* = 13.0 Hz, 1H), 6.54 (dd, *J* = 9.0,
299 2.6 Hz, 1H), 6.47 (d, *J* = 2.6 Hz, 1H), 5.84 (s, 1H), 5.21 (d, *J* = 13.0 Hz, 1H), 3.38 (q, *J* = 7.1
300 Hz, 4H), 2.97 (s, 6H), 1.18 (t, *J* = 7.1 Hz, 6H).

301 **7-(diethylamino)-2-oxo-2*H*-chromene-4-carbaldehyde** (**8)** was synthesized
302 according to the procedure described in the literature [23] and obtained as a dark red solid (21.0
303 g, quant.). Analytical data were in accordance with the literature. **R_f (*TLC conditions:***
304 **CH_2Cl_2:AcOEt, 95:5)**: 0.66 (Rev: DNP). **^{1}H NMR (300 MHz, $CDCl_3$) δ (ppm):** 10.01 (s,
305 1H), 8.28 (d, *J* = 9.2 Hz, 1H), 6.61 (dd, *J* = 9.2, 2.6 Hz, 1H), 6.50 (d, *J* = 2.6 Hz, 1H), 6.43 (s,
306 1H), 3.42 (q, *J* = 7.1 Hz, 4H), 1.21 (t, *J* = 7.1 Hz, 6H).

307 **7-(diethylamino)-4-(hydroxymethyl)-2*H*-chromen-2-one (9)** was synthesized
308 according to the procedure described in the literature [23] and obtained as a brown powder (15.0
309 g, 71 %°). Analytical data were in accordance with the literature. **R_f (*TLC conditions:***
310 **CH_2Cl_2:AcOEt, 95:5)**: 0.14 (Rev: UV). **^{1}H NMR ($CDCl_3$, 300 MHz), δ (ppm):** 7.30 (d, *J* =
311 9.0 Hz, 1H), 6.54 (dd, *J* = 9.0, 2.6 Hz, 1H), 6.45 (d, *J* = 2.6 Hz, 1H), 6.27 (t, *J* = 1.1 Hz, 1H),
312 4.82 (dd, *J* = 5.7, 1.1 Hz, 2H), 3.38 (q, *J* = 7.1 Hz, 4H), 2.96 (t, *J* = 5.7 Hz, 1H), 1.18 (t, *J* = 7.1
313 Hz, 6H).

314 **7-(diethylamino)-4-(hydroxymethyl)-3-iodo-2*H*-chromen-2-one (6)** was
315 synthesized according to the procedure described in the literature [23] and obtained as a dark
316 yellow powder (18.1 g, 70 %°). Analytical data were in accordance with the literature. **R_f (*TLC*
317 ***conditions:* CH_2Cl_2:AcOEt, 9:1)**: 0.60 (Rev: UV). **^{1}H NMR (acetone-d_6, 300 MHz), δ (ppm):**
318 7.85 (d, *J* = 9.2 Hz, 1H), 6.74 (dd, *J* = 9.2, 2.6 Hz, 1H), 6.52 (d, *J* = 2.6 Hz, 1H), 4.97 (d, *J* =
319 5.9 Hz, 2H), 4.67 (t, *J* = 5.9 Hz, 1H), 3.52 (q, *J* = 7.1 Hz, 4H), 1.22 (t, *J* = 7.1 Hz, 6H).

320

^{T}COUM$^{[OH]}$. Compound **4** (100 mg, 0.309 mmol, 1 eq.), compound **6** (381 mg, 1.02 mmol, 3.3 eq.), LiCl (45 mg, 1.09 mmol, 3.4 eq.), *n*Bu_4NCl (189 mg, 0.679 mmol, 2.2 eq.) and $NaHCO_3$ (117 mg, 1.39 mmol, 4.5 eq.) were dissolved in dry DMF (5 mL) under argon atmosphere. The mixture was degassed for 30 min with argon and $Pd(OAc)_2$ (7 mg, 3.09 µmol, 0.1 eq.) was added. The reaction mixture was stirred at 130 °C and carefully followed by TLC until total conversion of the starting material. Water was added and the mixture was extracted with AcOEt. The organic layer was dried with Na_2SO_4, filtered over Celite® and concentrated. The crude was purified by column chromatography of silicagel (eluent: CH_2Cl_2 100 % to CH_2Cl_2:AcOEt, 50:50) to give **^{T}COUM$^{[OH]}$** as an orange powder (130 mg, 40 %). **R_f (*TLC conditions:* CH_2Cl_2:AcOEt, 90:10)**: 0.11 (Rev: UV). **^{1}H NMR (300 MHz, DMSO-*d*$_6$) δ (ppm):** 7.73 (d, *J* = 9.4 Hz, 3H), 7.56 (d, *J* = 16.1 Hz, 3H), 7.53 (d, *J* = 8.5 Hz, 6H), 7.21 (d, *J* = 16.1 Hz, 3H), 7.07 (d, *J* = 8.5 Hz, 6H), 6.75 (dd, *J* = 9.4, 2.4 Hz, 3H), 6.53 (d, *J* = 2.4 Hz, 3H), 4.77 (s, 6H), 3.44 (t, *J* = 7.4 Hz, 12H), 1.14 (t, *J* = 7.4 Hz, 18H). **^{13}C NMR (76 MHz, DMSO) δ (ppm):** 160.4, 154.6, 149.9, 148.5, 146.1, 132.7, 132.0, 124.7, 123.9, 115.3, 109.1, 108.1, 96.4, 55.8, 44.0, 12.4. **HRMS (ESI)**: m/z = 1081.47213, calcd for $C_{66}H_{66}O_9N_4Na$ $(M+Na)^+$: 1081.47220 **FTIR ν (cm^{-1}):** 3394.1, 2974.7, 2963.1, 2924.5, 2897.5, 2875.3, 1688.4, 1604.5, 1501.3, 1411.6, 1354.8, 1315.2, 1263.2, 1143.6, 1077.1, 819.6, 773.3. **Melting point:** 151 °C

^{T}COUM$^{[Gly-Fmoc]}$. **^{T}COUM$^{[OH]}$** (50 mg, 47.2 µmol, 1 eq.) was added to a stirred solution of EDC.HCl (45 mg, 0.236 mmol, 5 eq.), DMAP (17 mg, 0.142 mmol, 3 eq.) and Fmoc-Gly-OH (70 mg, 0.236 mmol, 5 eq.) in dry CH_2Cl_2 (2 mL) under argon atmosphere. The solution was stirred in the dark for 48 h at room temperature. The mixture was directly loaded on a short column chromatography of silicagel (eluent: CH_2Cl_2 to CH_2Cl_2: AcOEt 80:20, step 5%) to give **^{T}COUM$^{[Gly-Fmoc]}$** as an orange powder (44.6 mg, 50 %). **R_f (*TLC conditions:* CH_2Cl_2:AcOEt, 9:1)**: 0.51 (Rev: UV). **^{1}H NMR (300 MHz, Chloroform-*d*) δ (ppm):** 7.72 (d, *J* = 7.4 Hz, 6H),

7.56 (d, *J* = 16.5 Hz, 3H), 7.51 (d, *J* = 7.4 Hz, 6H), 7.43 (d, *J* = 8.4 Hz, 6H), 7.36 (t, *J* = 7.4 Hz, 6H), 7.25 (t, *J* = 7.4 Hz, 6H), 7.17 – 7.13 (m, 6H), 7.08 (d, *J* = 8.4 Hz, 6H), 6.58 (dd, *J* = 9.2, 2.5 Hz, 3H), 6.43 (d, *J* = 2.5 Hz, 3H), 5.48 (s, 6H), 5.37 – 5.25 (m, 3H), 4.33 (d, *J* = 7.1 Hz, 6H), 4.12 (t, *J* = 7.1 Hz, 3H), 4.04 (d, *J* = 5.8 Hz, 6H), 3.36 (q, *J* = 7.5 Hz, 12H), 1.18 (d, *J* = 7.5 Hz, 18H). **^{13}C NMR (76 MHz, $CDCl_3$) δ (ppm):** 184.0, 174.0, 169.7, 160.9, 156.3, 154.7, 150.1, 147.0, 143.7, 141.2, 134.9, 127.9, 127.7, 127.0, 125.8, 125.1, 124.3, 120.0, 119.1, 109.2, 108.3, 97.4, 80.9, 67.3, 59.5, 47.0, 44.8, 42.9, 29.7, 14.1, 12.5. **HRMS (ESI)**: m/z = 970.86504, calcd for $C_{117}H_{105}O_{18}N_7Na_2$ $(M+Na)^{2+}$: 970.86503. **FTIR ν (cm^{-1}):** 3063.4, 3031.6, 2966.0, 2923.6, 2870.5, 1711.5, 1605.5, 1520.6, 1501.3, 1413.6, 1260.3, 1168.7, 1144.6, 739.6. **Melting point:** 134 °C.

***N,N*-diphenyl-4-vinylaniline (2).** Methyltriphenylphosphonium bromide (1.44 g, 4.02 mmol, 1.1 eq.) was dried under high vacuum with appropriate heating then purged and refilled with argon. Freshly distilled THF was added and argon was bubbled into the mixture for 15 min. *t*BuOK (452 mg, 4.02 mmol, 1.1 eq.) was added at 0 °C and the resulting mixture was stirred for 1 h at 0 °C. **1** (1 g, 3.66 mmol, 1 eq.) in solution in dry THF was then added dropwise and the mixture was stirred for 24 h at room temperature. Saturated aqueous NH_4Cl was added to quench the reaction and the mixture was extracted with Et_2O. The combined organic layers were dried with Na_2SO_4, filtered over Celite® and concentrated under reduced pressure. The crude was purified by flash chromatography on silicagel (eluent: AcOEt/PE, 5/95) to give the pure product **2** as a whitish oil (413 mg, 42 %). **R_f (*TLC conditions:* PE:AcOEt, 95:5)**: 0.83 (Rev: UV). **^{1}H NMR (300 MHz, Chloroform-*d*) δ (ppm)** 7.34 – 7.24 (m, 6H), 7.15 – 7.10 (m, 3H), 7.10 – 7.01 (m, 3H), 6.69 (dd, *J* = 17.6, 10.9 Hz, 1H), 5.67 (dd, *J* = 17.6, 1.0 Hz, 1H), 5.18 (dd, *J* = 10.9, 1.0 Hz, 1H). **^{13}C NMR (76 MHz, $CDCl_3$) δ (ppm)** 147.6, 147.5, 136.3, 131.9, 129.3, 127.1, 124.4, 123.7, 123.0, 112.2. **HRMS (ESI)**: m/z = 272.14305, calcd for $C_{20}H_{18}N$ $(M+H)^+$: 272.14338. **FTIR ν (cm^{-1}):** 3083.6, 3060.5, 3031.6, 2999.7, 2961.2, 2922.6, 2852.2,

1587.1, 1505.2, 1484.9, 1326.8, 1282.4, 1265.1, 1175.4, 838.9, 756.0, 697.1. **Melting point:** 107 °C.

^{M}COUM$^{[OH]}$. Compound **6** (100 mg, 0.268 mmol, 1 eq.), compound **2** (87 mg, 0.322 mmol, 1.2 eq.), LiCl (19 mg, 0.456 mmol, 1.7 eq.), *n*Bu_4NCl (82 mg, 0.295 mmol, 1.1 eq.) and $NaHCO_3$ (68 mg, 0.804 mmol, 3 eq.) were dissolved in dry DMF (5 mL) under argon atmosphere. The mixture was degassed for 30 min with argon and $Pd(OAc)_2$ (7 mg, 26.8 μmol, 0.1 eq.) was added. The reaction mixture was stirred at 130 °C and carefully followed by TLC until total conversion of the starting material. Water was added to quench the reaction and the mixture was extracted with AcOEt. The organic layer was dried over Na_2SO_4, filtered over Celite® and concentrated. The crude was purified by column chromatography of silicagel (eluent: CH_2Cl_2 100 % to CH_2Cl_2:AcOEt, 9:1) to give **^{M}COUM$^{[OH]}$** as a brown powder. (78 mg, 57 %). **R_f (*TLC conditions:* CH_2Cl_2:AcOEt, 9:1)**: 0.86 (Rev: UV). **^{1}H NMR (300 MHz, Chloroform-*d*) δ (ppm):** 7.67 (d, *J* = 9.1 Hz, 1H), 7.50 (d, *J* = 16.1 Hz, 1H), 7.39 (d, *J* = 8.7 Hz, 2H), 7.30 – 7.22 (m, 4H), 7.15 – 7.08 (m, 6H), 7.07 – 6.99 (m, 3H), 6.70 (d, *J* = 9.1 Hz, 1H), 6.55 (s, 1H), 4.96 (s, 2H), 3.41 (q, *J* = 7.3 Hz, 4H), 1.21 (t, *J* = 7.3 Hz, 6H). **^{13}C NMR (76 MHz, DMSO) δ (ppm):** 161.5, 147.7, 147.5, 145.4, 143.9, 131.8, 131.7, 129.3, 129.1, 127.7, 126.4, 124.6, 124.2, 123.3, 123.1, 119.6, 118.7, 109.6, 90.7, 57.8, 29.7, 12.4. **HRMS (ESI)**: m/z = 539.2302, calcd for $C_{34}H_{32}O_3N_2Na$ $(M+Na)^+$: 539.23051. **FTIR ν (cm^{-1}):** 3390.2, 2979.5, 1959.2, 2895.6, 2857.0, 1679.7, 1609.3, 1588.1, 1502.3, 1488.8, 753.1, 695.2. **Melting point:** 128 °C.

^{M}COUM$^{[Gly-Fmoc]}$. **^{M}COUM$^{[OH]}$** (50 mg, 96.8 μmol, 1 eq.) was added to a stirred solution of EDC.HCl (28 mg, 0.145 mmol, 1.5 eq.), DMAP (12 mg, 96.8 μmol, 1 eq.) and Fmoc-Gly-OH (43 mg, 0.145 mmol, 1.5 eq.) in dry CH_2Cl_2 (2.5 mL) under argon atmosphere. The solution was stirred in the dark for 48 h at room temperature. The mixture was directly loaded on a short column chromatography of silicagel (eluent: Toluene 100 % to

Toluene:AcOEt 80:20, step 5%) to give **^{M}COUM$^{[Gly\text{-}Fmoc]}$** as an orange powder (41.8 mg, 55 %). **R_f (*TLC conditions:* Toluene:AcOEt, 8:2)**: 0.71 (Rev: UV). **^{1}H NMR (300 MHz, Chloroform-*d*) δ (ppm):** 7.75 (d, *J* = 7.6 Hz, 2H), 7.58 – 7.49 (m, 4H), 7.41 (d, *J* = 8.4 Hz, 1H), 7.47 – 7.34 (m, 6H), 7.30 – 7.21 (m, 4H), 7.14 – 6.99 (m, 10H), 6.58 (dd, *J* = 9.1, 2.5 Hz, 1H), 6.44 (d, *J* = 2.5 Hz, 1H), 5.49 (s, 0H), 5.30 (t, *J* = 5.8 Hz, 1H), 4.35 (d, *J* = 7.1 Hz, 2H), 4.15 (t, *J* = 7.1 Hz, 1H), 4.06 (d, *J* = 5.8 Hz, 2H), 3.36 (q, *J* = 7.1 Hz, 4H), 1.18 (t, *J* = 7.1 Hz, 6H). **^{13}C NMR (76 MHz, $CDCl_3$) δ (ppm):** 169.8, 161.1, 156.4, 154.8, 150.2, 147.9, 147.6, 143.8, 141.4, 140.3, 135.2, 131.7, 129.4, 127.9, 127.8, 127.2, 125.9, 125.2, 124.8, 123.4, 123.3, 120.1, 119.4, 118.6, 109.3, 108.4, 97.5, 67.5, 59.8, 47.1, 44.9, 43.0, 29.8, 12.6. **HRMS (ESI)**: m/z = 818.31941, calcd for $C_{51}H_{45}O_6N_3Na$ $(M+Na)^+$: 818.32006. **FTIR ν (cm^{-1}):** 3060.5, 3036.4, 2972.7, 2964.1, 2918.7, 2872.5, 2849.3, 1708.6, 1608.3, 1587.1, 1504.2, 1488.8, 1412.6, 1260.3, 1168.7, 1144.6. **Melting point:** 117 °C.

Quantum chemical calculations

Molecular structures were optimized at the DFT level in the gas phase using the range-separated CAM-B3LYP exchange-correlation functional [36] in association with the 6-311G(d) Gaussian basis set. Dispersion effects were added by using the Grimme's D3 correction with Becke-Johnson damping (GD3BJ).[37] Vertical transition energies and excited state properties were computed by employing the Time-Dependent Density Functional Theory (TD-DFT) at the CAM-B3LYP/6-311G(d) level. Solvent effects (DMF) were taken into account in the calculations of optical properties by using the non-equilibrium Polarizable Continuum Model (PCM) in its integral equation formalism (IEF).[38] All calculations were performed using the Gaussian16 package.[39]

ACKNOWLEDGMENTS

We thank the University of Bordeaux for PhD fellowship to M.K. and V.D. M.B-D. acknowledges support from Conseil Régional d'Aquitaine (Chaire d'excellence). Calculations were performed on the HPC resources of the Institut des Sciences Moléculaires, co-funded by the Nouvelle Aquitaine region, as well as on the MCIA (Mésocentre de Calcul Intensif Aquitain) facilities of the Université de Bordeaux and of the Université de Pau et des Pays de l'Adour.

REFERENCES

[1] Klán P, Šolomek T, Bochet CG, Blanc A, Givens R, Rubina M, et al. Photoremovable Protecting Groups in Chemistry and Biology: Reaction Mechanisms and Efficacy. Chem Rev 2013;113:119–91. https://doi.org/10.1021/cr300177k.

[2] Mayer G, Heckel A. Biologically Active Molecules with a "Light Switch." Angew Chem Int Ed 2006;45:4900–21. https://doi.org/10.1002/anie.200600387.

[3] Ellis-Davies GCR. Caged compounds: photorelease technology for control of cellular chemistry and physiology. Nat Methods 2007;4:619–28. https://doi.org/10.1038/nmeth1072.

[4] Kaplan JH, Forbush B, Hoffman JF. Rapid photolytic release of adenosine 5'-triphosphate from a protected analog: utilization by the sodium:potassium pump of human red blood cell ghosts. Biochemistry 1978;17:1929–35. https://doi.org/10.1021/bi00603a020.

[5] Furuta T, Wang SS-H, Dantzker JL, Dore TM, Bybee WJ, Callaway EM, et al. Brominated 7-hydroxycoumarin-4-ylmethyls: photolabile protecting groups with biologically useful cross-sections for two photon photolysis. Proc Natl Acad Sci 1999;96:1193–200.

[6] Matsuzaki M, Ellis-Davies GCR, Nemoto T, Miyashita Y, Iino M, Kasai H. Dendritic spine geometry is critical for AMPA receptor expression in hippocampal CA1 pyramidal neurons. Nat Neurosci 2001;4:1086–92. https://doi.org/10.1038/nn736.

[7] Fedoryak OD, Dore TM. Brominated Hydroxyquinoline as a Photolabile Protecting Group with Sensitivity to Multiphoton Excitation. Org Lett 2002;4:3419–22. https://doi.org/10.1021/ol026524g.

[8] Nikolenko V, Yuste R, Zayat L, Baraldo LM, Etchenique R. Two-photon uncaging of neurochemicals using inorganic metal complexes. Chem Commun 2005:1752. https://doi.org/10.1039/b418572b.

[9] Brieke C, Rohrbach F, Gottschalk A, Mayer G, Heckel A. Light-Controlled Tools. Angew Chem Int Ed 2012;51:8446–76. https://doi.org/10.1002/anie.201202134.
[10] Bort G, Gallavardin T, Ogden D, Dalko PI. From One-Photon to Two-Photon Probes: "Caged" Compounds, Actuators, and Photoswitches. Angew Chem Int Ed 2013;52:4526–37. https://doi.org/10.1002/anie.201204203.
[11] Zhu Y, Pavlos CM, Toscano JP, Dore TM. 8-Bromo-7-hydroxyquinoline as a Photoremovable Protecting Group for Physiological Use: Mechanism and Scope. J Am Chem Soc 2006;128:4267–76. https://doi.org/10.1021/ja0555320.
[12] I. Kiskin, Rod Chillingworth, James N. The efficiency of two-photon photolysis of a "caged" fluorophore, o -1-(2-nitrophenyl)ethylpyranine, in relation to photodamage of synaptic terminals. Eur Biophys J 2002;30:588–604. https://doi.org/10.1007/s00249-001-0187-x.
[13] Abe M, Chitose Y, Jakkampudi S, Thuy P, Lin Q, Van B, et al. Design and Synthesis of Two-Photon Responsive Chromophores for Near-Infrared Light-Induced Uncaging Reactions. Synthesis 2017;49:3337–46. https://doi.org/10.1055/s-0036-1590813.
[14] Jakkampudi S, Abe M. Caged Compounds for Two-Photon Uncaging. Ref. Module Chem. Mol. Sci. Chem. Eng., Elsevier; 2018, p. B9780124095472136000. https://doi.org/10.1016/B978-0-12-409547-2.13667-4.
[15] Klausen M, Blanchard-Desce M. Two-photon uncaging of bioactive compounds: Starter guide to an efficient IR light switch. J Photochem Photobiol C Photochem Rev 2021:100423. https://doi.org/10.1016/j.jphotochemrev.2021.100423.
[16] Roy B, Roy S, Kundu M, Maji S, Pal B, Mandal M, et al. Ground-State Proton-Transfer (GSPT)-Assisted Enhanced Two-Photon Uncaging from a Binol-based AIE-Fluorogenic Phototrigger. Org Lett 2021;23:2308–13. https://doi.org/10.1021/acs.orglett.1c00445.
[17] Weinstain R, Slanina T, Kand D, Klán P. Visible-to-NIR-Light Activated Release: From Small Molecules to Nanomaterials. Chem Rev 2020:acs.chemrev.0c00663. https://doi.org/10.1021/acs.chemrev.0c00663.
[18] Fournier L, Aujard I, Le Saux T, Maurin S, Beaupierre S, Baudin J-B, et al. Coumarinylmethyl Caging Groups with Redshifted Absorption. Chem - Eur J 2013;19:17494–507. https://doi.org/10.1002/chem.201302630.

[19] Olson JP, Kwon H-B, Takasaki KT, Chiu CQ, Higley MJ, Sabatini BL, et al. Optically Selective Two-Photon Uncaging of Glutamate at 900 nm. J Am Chem Soc 2013;135:5954–7. https://doi.org/10.1021/ja4019379.
[20] Lin Q, Yang L, Wang Z, Hua Y, Zhang D, Bao B, et al. Coumarin Photocaging Groups Modified with an Electron-Rich Styryl Moiety at the 3-Position: Long-Wavelength Excitation, Rapid Photolysis, and Photobleaching. Angew Chem Int Ed 2018;57:3722–6. https://doi.org/10.1002/anie.201800713.
[21] Hagen V, Dekowski B, Nache V, Schmidt R, Geißler D, Lorenz D, et al. Coumarinylmethyl Esters for Ultrafast Release of High Concentrations of Cyclic Nucleotides upon One- and Two-Photon Photolysis. Angew Chem Int Ed 2005;44:7887–91. https://doi.org/10.1002/anie.200502411.
[22] Chaud J, Morville C, Bolze F, Garnier D, Chassaing S, Blond G, et al. Two-Photon Sensitive Coumarinyl Photoremovable Protecting Groups with Rigid Electron-Rich Cycles Obtained by Domino Reactions Initiated by a 5-*exo* -Dig Cyclocarbopalladation. Org Lett 2021;23:7580–5. https://doi.org/10.1021/acs.orglett.1c02778.
[23] Klausen M, Dubois V, Clermont G, Tonnelé C, Castet F, Blanchard-Desce M. Dual-wavelength efficient two-photon photorelease of glycine by π-extended dipolar coumarins. Chem Sci 2019;10:4209–19. https://doi.org/10.1039/C9SC00148D.
[24] Terenziani F, Katan C, Badaeva E, Tretiak S, Blanchard-Desce M. Enhanced Two-Photon Absorption of Organic Chromophores: Theoretical and Experimental Assessments. Adv Mater 2008;20:4641–78. https://doi.org/10.1002/adma.200800402.
[25] Picard S, Genin E, Clermont G, Hugues V, Mongin O, Blanchard-Desce M. Octupolar chimeric compounds built from quinoline caged acetate moieties: a novel approach for 2-photon uncaging of biomolecules. New J Chem 2013;37:3899. https://doi.org/10.1039/c3nj00833a.
[26] Dunkel P, Petit M, Dhimane H, Blanchard-Desce M, Ogden D, Dalko PI. Quinoline-Derived Two-Photon-Sensitive Octupolar Probes. ChemistryOpen 2017;6:660–7. https://doi.org/10.1002/open.201700097.
[27] Schade B, Hagen V, Schmidt R, Herbrich R, Krause E, Eckardt T, et al. Deactivation Behavior and Excited-State Properties of (Coumarin-4-yl)methyl Derivatives. 1. Photocleavage of (7-Methoxycoumarin-4-yl)methyl-Caged Acids with Fluorescence Enhancement. J Org Chem 1999;64:9109–17. https://doi.org/10.1021/jo9910233.

[28] Schmidt R, Geissler D, Hagen V, Bendig J. Kinetics Study of the Photocleavage of (Coumarin-4-yl)methyl Esters. J Phys Chem A 2005;109:5000–4. https://doi.org/10.1021/jp050581k.
[29] Nadler A, Yushchenko DA, Müller R, Stein F, Feng S, Mulle C, et al. Exclusive photorelease of signalling lipids at the plasma membrane. Nat Commun 2015;6:10056. https://doi.org/10.1038/ncomms10056.
[30] Jeffery T. On the efficiency of tetraalkylammonium salts in Heck type reactions. Tetrahedron 1996;52:10113–30. https://doi.org/10.1016/0040-4020(96)00547-9.
[31] Neises B, Steglich W. Simple Method for the Esterification of Carboxylic Acids. Angew Chem Int Ed Engl 1978;17:522–4. https://doi.org/10.1002/anie.197805221.
[32] Bojtár M, Kormos A, Kis-Petik K, Kellermayer M, Kele P. Green-Light Activatable, Water-Soluble Red-Shifted Coumarin Photocages. Org Lett 2019;21:9410–4. https://doi.org/10.1021/acs.orglett.9b03624.
[33] Bojtár M, Németh K, Domahidy F, Knorr G, Verkman A, Kállay M, et al. Conditionally Activatable Visible-Light Photocages. J Am Chem Soc 2020;142:15164–71. https://doi.org/10.1021/jacs.0c07508.
[34] Grabowski ZR, Rotkiewicz K, Rettig W. Structural Changes Accompanying Intramolecular Electron Transfer: Focus on Twisted Intramolecular Charge-Transfer States and Structures. Chem Rev 2003;103:3899–4032. https://doi.org/10.1021/cr940745l.
[35] Katan C, Tretiak S, Werts MHV, Bain AJ, Marsh RJ, Leonczek N, et al. Two-Photon Transitions in Quadrupolar and Branched Chromophores: Experiment and Theory. J Phys Chem B 2007;111:9468–83. https://doi.org/10.1021/jp071069x.
[36] Yanai T, Tew DP, Handy NC. A new hybrid exchange–correlation functional using the Coulomb-attenuating method (CAM-B3LYP). Chem Phys Lett 2004;393:51–7. https://doi.org/10.1016/j.cplett.2004.06.011.
[37] Grimme S, Ehrlich S, Goerigk L. Effect of the damping function in dispersion corrected density functional theory. J Comput Chem 2011;32:1456–65. https://doi.org/10.1002/jcc.21759.
[38] Tomasi J, Mennucci B, Cammi R. Quantum Mechanical Continuum Solvation Models. Chem Rev 2005;105:2999–3094. https://doi.org/10.1021/cr9904009.
[39] Frisch MJ, Trucks GW, Schlegel HB, Scuseria GE, Robb MA, Cheeseman JR, et al. Gaussian 16. Wallingford CT: Gaussian, Inc.; 2016.